

Kinetic freeze-out temperature and transverse flow velocity in Au-Au collisions at RHIC-BES energies

Muhammad Waqas*, Bao-Chun Li†

*Institute of Theoretical Physics & Department of Physics &
State Key Laboratory of Quantum Optics and Quantum Optics Devices,
Shanxi University, Taiyuan, Shanxi 030006, China*

Abstract: Based on the data-driven analysis, the mid-rapidity transverse momentum (p_T) spectra of charged hadrons (π^+ , K^+ and p) produced in central and peripheral gold-gold (Au-Au) collisions from the Beam Energy Scan (BES) program at the Relativistic Heavy Ion Collider (RHIC) are fitted by the blast-wave model with Boltzmann-Gibbs statistics. The model result are in agreement with the experimental data measured by the STAR Collaboration at the RHIC-BES energies. We observe that the kinetic freeze-out temperature (T_0), transverse flow velocity (β_T), mean transverse momentum ($\langle p_T \rangle$), and initial temperature (T_i) increase with the collision energy and with the event centrality.

Keywords: Kinetic freeze-out temperature, transverse flow velocity, mean transverse momentum, initial temperature, high energy collisions

PACS: 12.40.Ee, 13.85.Hd, 25.75.Ag, 25.75.Dw, 24.10.Pa

1 Introduction

One of the most fundamental questions in nuclear matter is to determine the phase structure of the strongly-interacting quantum chromodynamics (QCD) matter [1, 2, 3]. The yield ratios, transverse momentum (p_T) spectra and other data for various identified particles produced in proton-proton (pp), proton-nucleus (pA) and nucleus-nucleus (AA) collisions at high energies are important observable quantities for determining the phase structure. The experimental facilities, for example the Relativistic Heavy-Ion Collider (RHIC) and the Large Hadron Collider (LHC) provide excellent tools to study the properties of Quark-Gluon Plasma (QGP) [4, 5, 6].

The phase diagram of the QCD matter is usually expressed in terms of the chemical freeze-out temperature (T_{ch}) and the baryon chemical potential (μ_B) [7, 8]. Besides, other quantities such as the kinetic freeze-out temperature (T_{kin} or T_0) and transverse flow velocity (β_T) are useful to understand the phase diagram [9]. To search for the possible critical energy in the phase transition from hadronic matter to QGP in high energy collisions, the STAR Collaboration has been performing

the Beam Energy Scan (BES) program [10, 11, 12, 13] at the RHIC. Besides, other experiments at similar or lower energies at other accelerators are scheduled [14, 15].

Generally, the processes of high energy collisions result possibly in three main stages [16, 17, 18]:

- i) The initial stage: at this stage the collisions are in the beginning. The temperature at this stage is called the initial temperature which is one of the main factors to affect the particle spectra, which is less studied in the community comparatively. After the initial state, the “fireball” leads to a decrease in the temperature and finally to the hadronization.
- ii) The chemical freeze-out stage: at this stage the inner collisions among various particles are elastic and the yield ratios of differential types of particles remain invariant. The chemical freeze-out temperature T_{ch} can be obtained from the particle ratios, which is much studied in the community comparatively.
- iii) The kinetic freeze-out stage: at this stage the scattering processes stop and the hadrons decouple from the rest of the system and the hadron’s energy/momentum spectra freeze in time. The tem-

*E-mail: waqas_phy313@yahoo.com

†Corresponding author. E-mail: libc2010@163.com; s6109@sxu.edu.cn

perature at this stage is known as the kinetic freeze-out temperature T_0 which can be obtained from the p_T spectra.

When one studies T_0 from the p_T spectra, the effect of β_T should be eliminated. If the effect of β_T is not eliminated in the temperature, this temperature is called the effective temperature (T_{eff} or T). At the stage of kinetic freeze-out, T_0 and β_T are two important parameters which describe the thermal motion of the produced particles and the collective expansion of the emission source respectively. The spectra in low- p_T region ($p_T = 2\text{--}3$ GeV/ c) which is mainly contributed by the soft excitation process essentially separate the contribution of the thermal motion and the collective expansion, if one only extracts T_0 and β_T . The spectra in high- p_T region are contributed by the hard scattering process which is not needed in extracting T_0 and β_T .

We are very interested in the extraction of T_0 and β_T in collisions at the RHIC-BES energies which are very suitable to study the spectra in low- p_T region, where the spectra in high- p_T region are not produced due to not too high energies. In this work, the double differential p_T spectra of charged particles dependences on collision energy and event centrality in gold-gold (Au-Au) collisions are analyzed by the blast-wave model with Boltzmann-Gibbs statistics by means of data-driven analysis. The model results are compared with the data measured by the STAR Collaboration at the RHIC-BES energies [19, 20].

The remainder of this work consists of the method and formalism, results and discussion as well as conclusions. We shall describe the remanent parts orderly.

2 The method and formalism

Various methods can be used for the extraction of T_0 and β_T , e.g. the blast-wave model with Boltzmann-Gibbs statistics [21, 22, 23], the blast-wave model with Tsallis statistics [24, 25, 26], an alternative method by using the Boltzmann-Gibbs statistics [22, 27, 28, 29, 30, 31, 32, 33] and the alternative method by using Tsallis distribution [33, 34, 35, 36, 37, 38, 39]. In this work, we choose the blast-wave model with Boltzmann-Gibbs statistics due to its similarity with the ideal gas model in thermodynamics and few parameters. However, these methods only describe the spectra in low- p_T region. For the spectra in high- p_T region if available, the Hagedorn function which is known as the inverse power-law [40, 41]

can be used. We shall discuss these issues in detail as follows.

In general, there are two main processes responsible in the contribution of p_T spectra. They are i) the soft excitation process which contributes the soft component in low- p_T region and ii) the hard scattering process which contributes the hard component in high- p_T region.

For the soft component, according to refs. [21, 22, 23], the probability density function of the p_T spectra in the blast-wave model with Boltzmann-Gibbs statistics results in

$$f_1(p_T) = \frac{1}{N} \frac{dN}{dp_T} = C p_T m_T \int_0^R r dr \times I_0 \left[\frac{p_T \sinh(\rho)}{T_0} \right] K_1 \left[\frac{m_T \cosh(\rho)}{T_0} \right], \quad (1)$$

where N is the number of particles, C is the normalization constant, $m_T = \sqrt{p_T^2 + m_0^2}$ is the transverse mass, m_0 is the rest mass of the considered particle, r and R are the radial position and the maximum radial position respectively, I_0 and K_1 are the modified Bessel functions of the first and second kinds respectively, $\rho = \tanh^{-1}[\beta(r)]$ is the boost angle, $\beta(r) = \beta_S (r/R)^{n_0}$ is a self-similar flow profile, β_S is the flow velocity on the surface, and $n_0 = 2$ is used in original form [21]. Particularly, $\beta_T = (2/R^2) \int_0^R r \beta(r) dr = 2\beta_S / (n_0 + 2) = 0.5\beta_S$. The parameter n_0 is used different in different works, e.g. $n_0 = 1$ or non-integer in refs. [24, 42], which corresponds to the centrality from center to periphery.

Equation (1) and similar or related functions are not enough to describe the whole p_T spectra. In particular, the maximum p_T reaches up to 100 GeV/ c in collisions at the LHC [43]. Then, one needs other functions such as the Tsallis-Lévy [44, 45] or Tsallis-Pareto-type function [44, 46] and the Hagedorn function [40, 41] or inverse power law [47, 48, 49] to the spectra in high and very high- p_T regions. In this work, the hard component is simply represented by the inverse power law. That is

$$f_2(p_T) = \frac{1}{N} \frac{dN}{dp_T} = A p_T \left(1 + \frac{p_T}{p_0} \right)^{-n}, \quad (2)$$

where p_0 and n are free parameters and A is the normalization constant which is related to the free parameters.

However, the structure of p_T spectra is very complex. In fact, several regions have been observed and analyzed in ref. [50]. These regions include the first one with $p_T < 4\text{--}6$ GeV/ c , the second one with $4\text{--}6$ GeV/ $c < p_T < 17\text{--}20$ GeV/ c and the third one with $p_T > 17\text{--}20$ GeV/ c . Different regions maybe correspond to different mechanisms. The first p_T region in

our discussion is regarded as the region of soft excitation process, while the second and third p_T regions are regarded as the regions of hard and very hard excitation process respectively. In particular, a special region with $p_T < 0.2\text{--}0.3$ GeV/ c is considered due to the resonant production in some cases, and it is regarded as the region of very soft excitation process.

Generally, all the p_T regions discussed above can be unifiedly superposed by two methods: i) the general superposition in which the contribution regions of different components overlap each other and ii) the Hagedorn model (the usual step function) [40] in which there is no overlapping of different regions of different components.

Considering $f_1(p_T)$, $f_2(p_T)$, $f_{VS}(p_T)$ and $f_{VH}(p_T)$ which denote the probability density functions by the soft, hard, very soft and very hard components respectively, where $f_{VS}(p_T)$ and $f_{VH}(p_T)$ are assumed to be in the form of $f_1(p_T)$ and $f_2(p_T)$ respectively, the unified superposition according to the first method is

$$f_0(p_T) = \frac{1}{N} \frac{dN}{dp_T} = k_{VS} f_{VS}(p_T) + k f_1(p_T) + (1 - k - k_{VS} - k_{VH}) f_2(p_T) + k_{VH} f_{VH}(p_T), \quad (3)$$

where k_{VS} is the contribution fraction of very soft component, while k and k_{VH} denote the contributions of soft and very hard components respectively.

The step function can be used to structure the superposition according to Hagedorn model [40], i.e.

$$f_0(p_T) = \frac{1}{N} \frac{dN}{dp_T} = A_{VS} \theta(p_{VS} - p_T) f_{VS}(p_T) + A_1 \theta(p_T - p_{VS}) \theta(p_1 - p_T) f_1(p_T) + A_2 \theta(p_T - p_1) \theta(p_{VH} - p_T) f_2(p_T) + A_{VH} \theta(p_T - p_{VH}) f_{VH}(p_T), \quad (4)$$

where A_{VS} , A_1 , A_2 and A_{VH} are the constants which make the interfacing components link to each other perfectly.

Particularly, if the contributions of very soft and very hard components can be neglected, Eqs. (3) and (4) are simplified to be

$$f_0(p_T) = \frac{1}{N} \frac{dN}{dp_T} = k f_1(p_T) + (1 - k) f_2(p_T) \quad (5)$$

and

$$f_0(p_T) = \frac{1}{N} \frac{dN}{dp_T} = A_1 \theta(p_1 - p_T) f_1(p_T) + A_2 \theta(p_T - p_1) f_2(p_T) \quad (6)$$

respectively. Further, if the contribution of hard component at the RHIC-BES energies can be neglected, Eqs. (5) and (6) are simplified to be the same form

$$f_0(p_T) = \frac{1}{N} \frac{dN}{dp_T} = f_1(p_T). \quad (7)$$

This work deals with Au-Au collisions at the RHIC-BES energies, for which Eq. (7) i.e. Eq. (1) is suitable. In the following section, we shall use Eq. (1) to fit the experimental data measured by the STAR Collaboration at the RHIC-BES energies [19, 20].

3 Results and discussion

Figure 1 presents the event centrality dependent double differential p_T spectra, $(1/2\pi p_T) d^2N/dp_T dy$, of π^+ , K^+ and p produced in the mid-rapidity interval $|y| < 0.1$ in Au-Au collisions at the center-of-mass energy per nucleon pair $\sqrt{s_{NN}} = 7.7$ GeV at the RHIC-BES, where y denotes the rapidity. The symbols represent the experimental data measured by the STAR Collaboration [19] and the curves are our fitting results by using the blast-wave model with Boltzmann-Gibbs statistics, Eq. (1) [21, 22, 23]. The spectra in centrality class 0–5%, 5–10%, 10–20%, 20–30%, 30–40%, 40–50%, 50–60%, 60–70% and 70–80% are scaled by 1, 1/2, 1/4, 1/6, 1/8, 1/10, 1/12, 1/14 and 1/16 respectively. The related parameters along with χ^2 and degree of freedom (dof) are listed in Table 1, where the centrality classes are listed together. One can see that Eq. (1) fits well the data in Au-Au collisions at 7.7 GeV at the RHIC.

Figure 2 is the same as Fig. 1, but it shows the p_T spectra at $\sqrt{s_{NN}} = 11.5$ GeV. One can see that Eq. (1) fits well the data in Au-Au collisions at 11.5 GeV at the RHIC-BES.

Figure 3 is also the same as Fig. 1, but it shows the p_T spectra at $\sqrt{s_{NN}} = 14.5$ GeV, where the data are cited from ref. [20]. Once again, Eq. (1) fits well the data in Au-Au collisions at 14.5 GeV at the RHIC-BES.

Figures 4–6 are also the same as Fig. 1, but they show the p_T spectra at $\sqrt{s_{NN}} = 19.6$, 27 and 39 GeV, respectively. Once more, Eq. (1) fits well the data in Au-Au collisions at other RHIC-BES energies.

It is noteworthy to point out that Eq. (1) for the blast-wave model in the system is assumed to be in local thermodynamic equilibrium and therefore, a single T_0 and β_T should be obtained by the weight average of different particles species. To see clearly the trends of weight average parameters, Figs. 7(a) and 7(b) show the dependences of weight averages T_0 and β_T on $\sqrt{s_{NN}}$ for

Table 1. Values of free parameters (T_0 and β_T), normalization constant (N_0), χ^2 , and dof corresponding to the curves in Figs. 1–6.

Figure	Particle	Centrality	T_0	β_T	N_0	χ^2	dof	
Fig. 1 Au-Au 7.7 GeV	π^+	0–5%	0.130 ± 0.004	0.306 ± 0.006	15.00 ± 1.00	17	26	
		5–10%	0.129 ± 0.005	0.305 ± 0.005	6.02 ± 0.9	14	26	
		10–20%	0.128 ± 0.004	0.303 ± 0.007	2.35 ± 1.05	20	26	
		20–30%	0.126 ± 0.005	0.302 ± 0.006	1.09 ± 0.60	18	26	
		30–40%	0.124 ± 0.004	0.300 ± 0.006	0.54 ± 0.43	19	26	
		40–50%	0.122 ± 0.003	0.297 ± 0.007	0.28 ± 0.02	13	26	
		50–60%	0.120 ± 0.004	0.292 ± 0.004	0.14 ± 0.02	20	25	
		60–70%	0.118 ± 0.004	0.280 ± 0.005	0.067 ± 0.001	16	24	
	K^+	70–80%	0.115 ± 0.005	0.269 ± 0.007	0.030 ± 0.008	11	21	
		0–5%	0.133 ± 0.005	0.305 ± 0.005	3.65 ± 0.20	99	23	
		5–10%	0.131 ± 0.004	0.304 ± 0.005	1.50 ± 0.15	76	25	
		10–20%	0.130 ± 0.004	0.302 ± 0.007	0.53 ± 0.05	55	25	
		20–30%	0.128 ± 0.005	0.301 ± 0.007	0.24 ± 0.17	27	25	
		30–40%	0.127 ± 0.004	0.299 ± 0.009	0.11 ± 0.01	27	24	
		40–50%	0.125 ± 0.006	0.296 ± 0.008	0.050 ± 0.002	16	23	
		50–60%	0.123 ± 0.005	0.278 ± 0.007	0.23 ± 0.02	34	22	
	p	60–70%	0.118 ± 0.004	0.265 ± 0.008	0.0093 ± 0.0007	34	21	
		70–80%	0.116 ± 0.004	0.250 ± 0.008	0.0034 ± 0.0003	29	29	
		0–5%	0.134 ± 0.004	0.340 ± 0.005	9.31 ± 0.60	54	29	
		5–10%	0.133 ± 0.005	0.328 ± 0.006	3.90 ± 0.15	47	29	
		10–20%	0.132 ± 0.006	0.318 ± 0.008	1.50 ± 0.20	46	29	
		20–30%	0.130 ± 0.005	0.310 ± 0.008	0.65 ± 0.05	28	29	
		30–40%	0.128 ± 0.004	0.301 ± 0.006	0.32 ± 0.04	14	28	
		40–50%	0.126 ± 0.005	0.280 ± 0.007	0.15 ± 0.03	13	28	
	Fig. 2 Au-Au 11.5 GeV	π^+	50–60%	0.124 ± 0.004	0.271 ± 0.006	0.070 ± 0.008	7	27
			60–70%	0.122 ± 0.003	0.250 ± 0.005	0.030 ± 0.004	8	28
			70–80%	0.120 ± 0.006	0.204 ± 0.009	0.013 ± 0.001	14	21
			0–5%	0.132 ± 0.004	0.315 ± 0.005	19.11 ± 1.60	5	26
5–10%			0.130 ± 0.005	0.313 ± 0.005	7.60 ± 1.40	16	26	
10–20%			0.129 ± 0.004	0.312 ± 0.006	2.90 ± 0.50	14	26	
20–30%			0.128 ± 0.003	0.311 ± 0.007	1.36 ± 0.10	34	26	
30–40%			0.127 ± 0.003	0.310 ± 0.008	0.38 ± 0.05	15	26	
K^+		40–50%	0.126 ± 0.006	0.307 ± 0.007	0.34 ± 0.03	16	26	
		50–60%	0.124 ± 0.004	0.305 ± 0.005	0.16 ± 0.01	7	26	
		60–70%	0.121 ± 0.004	0.296 ± 0.006	0.080 ± 0.007	6	24	
		70–80%	0.119 ± 0.005	0.288 ± 0.008	0.040 ± 0.005	10	24	
		0–5%	0.135 ± 0.005	0.314 ± 0.009	4.23 ± 0.30	64	25	
		5–10%	0.133 ± 0.004	0.312 ± 0.008	1.72 ± 0.10	62	26	
		10–20%	0.132 ± 0.006	0.310 ± 0.010	0.60 ± 0.05	46	26	
		20–30%	0.130 ± 0.003	0.308 ± 0.004	0.27 ± 0.02	45	26	
p		30–40%	0.129 ± 0.004	0.307 ± 0.006	0.13 ± 0.01	59	26	
		40–50%	0.128 ± 0.005	0.306 ± 0.007	0.060 ± 0.006	11	26	
		50–60%	0.126 ± 0.004	0.300 ± 0.006	0.026 ± 0.002	15	25	
		60–70%	0.124 ± 0.003	0.288 ± 0.005	0.011 ± 0.001	6	23	
		70–80%	0.122 ± 0.004	0.264 ± 0.011	0.0050 ± 0.0003	26	22	
		0–5%	0.136 ± 0.005	0.323 ± 0.007	7.74 ± 1.00	55	28	
		5–10%	0.135 ± 0.005	0.321 ± 0.007	2.90 ± 0.25	56	29	
		10–20%	0.134 ± 0.005	0.318 ± 0.006	1.12 ± 0.15	40	29	
p		20–30%	0.132 ± 0.004	0.311 ± 0.007	0.50 ± 0.03	24	29	
		30–40%	0.130 ± 0.005	0.308 ± 0.007	0.24 ± 0.01	13	29	
		40–50%	0.128 ± 0.003	0.285 ± 0.006	0.12 ± 0.01	10	28	
		50–60%	0.125 ± 0.004	0.274 ± 0.008	0.55 ± 0.01	13	28	
	60–70%	0.123 ± 0.004	0.251 ± 0.006	0.024 ± 0.004	7	28		
	70–80%	0.121 ± 0.004	0.231 ± 0.007	0.010 ± 0.003	23	29		

Table 1. Continued.

Figure	Particle	Centrality	T_0	β_T	N_0	χ^2	dof
Fig. 3 Au-Au 14.5 GeV	π^+	0-5%	0.135 ± 0.003	0.320 ± 0.005	22.14 ± 2.00	4	28
		5-10%	0.133 ± 0.003	0.318 ± 0.006	8.50 ± 2.00	10	28
		10-20%	0.132 ± 0.004	0.317 ± 0.006	3.50 ± 0.25	12	28
		20-30%	0.131 ± 0.004	0.315 ± 0.005	1.60 ± 0.13	15	28
		30-40%	0.130 ± 0.004	0.314 ± 0.007	0.80 ± 0.06	10	28
		40-50%	0.128 ± 0.004	0.311 ± 0.006	0.40 ± 0.03	16	28
		50-60%	0.126 ± 0.004	0.307 ± 0.007	0.19 ± 0.02	7	28
		60-70%	0.124 ± 0.004	0.299 ± 0.007	0.093 ± 0.014	8	28
	70-80%	0.120 ± 0.005	0.291 ± 0.005	0.040 ± 0.006	14	28	
	K^+	0-5%	0.137 ± 0.005	0.318 ± 0.007	4.36 ± 0.40	16	26
		5-10%	0.136 ± 0.004	0.314 ± 0.008	1.86 ± 0.20	8	26
		10-20%	0.135 ± 0.005	0.313 ± 0.008	0.70 ± 0.08	21	26
		20-30%	0.134 ± 0.004	0.312 ± 0.006	0.31 ± 0.03	15	26
		30-40%	0.132 ± 0.004	0.310 ± 0.009	0.14 ± 0.01	9	26
		40-50%	0.130 ± 0.003	0.308 ± 0.008	0.067 ± 0.006	7	24
50-60%		0.128 ± 0.006	0.305 ± 0.010	0.025 ± 0.003	9	24	
60-70%		0.127 ± 0.004	0.294 ± 0.007	0.012 ± 0.001	3	22	
p	0-5%	0.139 ± 0.005	0.335 ± 0.009	6.47 ± 0.70	22	25	
	5-10%	0.137 ± 0.004	0.328 ± 0.008	2.90 ± 0.30	20	25	
	10-20%	0.135 ± 0.003	0.326 ± 0.008	1.03 ± 0.12	18	25	
	20-30%	0.134 ± 0.004	0.323 ± 0.007	0.46 ± 0.07	15	25	
	30-40%	0.132 ± 0.004	0.315 ± 0.008	0.21 ± 0.03	12	25	
	40-50%	0.130 ± 0.005	0.311 ± 0.007	0.096 ± 0.012	11	25	
	50-60%	0.128 ± 0.005	0.294 ± 0.005	0.042 ± 0.007	13	25	
	60-70%	0.126 ± 0.005	0.270 ± 0.008	0.018 ± 0.004	18	25	
70-80%	0.123 ± 0.004	0.236 ± 0.007	0.0080 ± 0.0019	26	25		
Fig. 4 Au-Au 19.6 GeV	π^+	0-5%	0.138 ± 0.004	0.322 ± 0.004	24.14 ± 2.00	9	26
		5-10%	0.137 ± 0.004	0.321 ± 0.005	9.50 ± 0.80	6	26
		10-20%	0.135 ± 0.005	0.319 ± 0.008	3.75 ± 0.25	7	26
		20-30%	0.134 ± 0.004	0.317 ± 0.005	1.97 ± 0.16	12	26
		30-40%	0.132 ± 0.003	0.315 ± 0.005	0.87 ± 0.06	18	26
		40-50%	0.130 ± 0.004	0.312 ± 0.006	0.43 ± 0.04	20	26
		50-60%	0.129 ± 0.005	0.311 ± 0.008	0.22 ± 0.02	16	26
		60-70%	0.128 ± 0.004	0.308 ± 0.008	0.10 ± 0.01	16	26
	70-80%	0.125 ± 0.005	0.303 ± 0.009	0.048 ± 0.004	14	26	
	K^+	0-5%	0.140 ± 0.003	0.320 ± 0.007	4.98 ± 0.30	24	26
		5-10%	0.138 ± 0.005	0.319 ± 0.009	2.00 ± 0.20	33	26
		10-20%	0.136 ± 0.005	0.318 ± 0.007	0.75 ± 0.05	33	26
		20-30%	0.135 ± 0.005	0.314 ± 0.007	0.34 ± 0.02	21	26
		30-40%	0.133 ± 0.004	0.311 ± 0.007	0.16 ± 0.03	12	26
		40-50%	0.130 ± 0.005	0.309 ± 0.009	0.075 ± 0.005	15	26
50-60%		0.129 ± 0.004	0.307 ± 0.008	0.036 ± 0.005	8	26	
60-70%		0.128 ± 0.006	0.300 ± 0.010	0.016 ± 0.001	23	26	
70-80%	0.126 ± 0.004	0.294 ± 0.009	0.0070 ± 0.0003	25	26		
p	0-5%	0.142 ± 0.005	0.338 ± 0.006	5.84 ± 0.70	41	29	
	5-10%	0.140 ± 0.006	0.336 ± 0.008	2.40 ± 0.30	28	25	
	10-20%	0.138 ± 0.005	0.334 ± 0.005	0.91 ± 0.12	19	23	
	20-30%	0.136 ± 0.005	0.324 ± 0.007	0.37 ± 0.06	41	23	
	30-40%	0.133 ± 0.004	0.316 ± 0.005	0.18 ± 0.03	20	23	
	40-50%	0.131 ± 0.006	0.312 ± 0.008	0.090 ± 0.016	8	23	
	50-60%	0.129 ± 0.005	0.295 ± 0.009	0.042 ± 0.007	14	23	
	60-70%	0.128 ± 0.004	0.275 ± 0.008	0.019 ± 0.003	2	23	
70-80%	0.125 ± 0.004	0.237 ± 0.007	0.0080 ± 0.0013	11	23		

Table 1. Continued.

Figure	Particle	Centrality	T_0	β_T	N_0	χ^2	dof
Fig. 5 Au-Au 27 GeV	π^+	0-5%	0.139 ± 0.004	0.326 ± 0.006	26.14 ± 1.80	5	26
		5-10%	0.138 ± 0.004	0.324 ± 0.008	11.07 ± 2.00	8	26
		10-20%	0.136 ± 0.005	0.323 ± 0.004	4.25 ± 0.25	10	26
		20-30%	0.135 ± 0.004	0.322 ± 0.004	1.90 ± 0.15	14	26
		30-40%	0.133 ± 0.003	0.321 ± 0.004	0.98 ± 0.10	23	26
		40-50%	0.131 ± 0.004	0.320 ± 0.006	0.50 ± 0.03	26	26
		50-60%	0.130 ± 0.005	0.318 ± 0.005	0.23 ± 0.03	19	26
		60-70%	0.129 ± 0.005	0.317 ± 0.009	0.11 ± 0.01	21	26
		70-80%	0.128 ± 0.004	0.315 ± 0.005	0.048 ± 0.005	19	26
	K^+	0-5%	0.142 ± 0.005	0.324 ± 0.008	5.11 ± 0.60	53	26
		5-10%	0.140 ± 0.005	0.322 ± 0.007	2.15 ± 0.20	52	26
		10-20%	0.139 ± 0.003	0.321 ± 0.008	0.82 ± 0.10	55	26
		20-30%	0.137 ± 0.006	0.321 ± 0.005	0.37 ± 0.03	43	26
		30-40%	0.136 ± 0.004	0.320 ± 0.007	0.18 ± 0.01	25	26
		40-50%	0.134 ± 0.004	0.318 ± 0.008	0.86 ± 0.01	9	26
		50-60%	0.132 ± 0.005	0.316 ± 0.005	0.040 ± 0.005	8	26
		60-70%	0.130 ± 0.004	0.311 ± 0.006	0.014 ± 0.003	12	26
		70-80%	0.128 ± 0.004	0.304 ± 0.007	0.0070 ± 0.0004	27	26
	p	0-5%	0.144 ± 0.004	0.343 ± 0.007	5.31 ± 0.40	34	23
		5-10%	0.143 ± 0.004	0.341 ± 0.007	2.20 ± 0.22	27	23
		10-20%	0.141 ± 0.005	0.336 ± 0.007	0.84 ± 0.09	21	23
20-30%		0.139 ± 0.005	0.330 ± 0.006	0.37 ± 0.05	15	23	
30-40%		0.137 ± 0.005	0.326 ± 0.008	0.18 ± 0.03	9	23	
40-50%		0.134 ± 0.005	0.318 ± 0.005	0.090 ± 0.016	8	23	
50-60%		0.131 ± 0.004	0.300 ± 0.008	0.042 ± 0.005	3	23	
60-70%		0.129 ± 0.004	0.280 ± 0.005	0.019 ± 0.002	6	23	
70-80%		0.126 ± 0.004	0.257 ± 0.007	0.0070 ± 0.0003	9	23	
Fig. 6 Au-Au 39 GeV	π^+	0-5%	0.141 ± 0.004	0.330 ± 0.007	27.84 ± 2.30	7	26
		5-10%	0.139 ± 0.005	0.328 ± 0.007	11.60 ± 0.70	14	26
		10-20%	0.138 ± 0.004	0.326 ± 0.006	4.50 ± 0.30	23	26
		20-30%	0.136 ± 0.004	0.325 ± 0.005	2.12 ± 0.10	38	26
		30-40%	0.135 ± 0.003	0.324 ± 0.008	1.05 ± 0.08	42	26
		40-50%	0.135 ± 0.005	0.322 ± 0.005	0.52 ± 0.02	36	26
		50-60%	0.134 ± 0.004	0.321 ± 0.008	0.27 ± 0.02	39	26
		60-70%	0.132 ± 0.004	0.320 ± 0.007	0.12 ± 0.01	36	26
		70-80%	0.130 ± 0.005	0.319 ± 0.008	0.062 ± 0.005	51	26
	K^+	0-5%	0.148 ± 0.004	0.328 ± 0.005	5.29 ± 0.40	35	26
		5-10%	0.147 ± 0.004	0.327 ± 0.006	2.30 ± 0.15	15	26
		10-20%	0.146 ± 0.005	0.328 ± 0.005	0.90 ± 0.08	29	26
		20-30%	0.145 ± 0.006	0.324 ± 0.009	0.40 ± 0.03	19	26
		30-40%	0.144 ± 0.005	0.323 ± 0.008	0.19 ± 0.01	12	26
		40-50%	0.143 ± 0.005	0.321 ± 0.006	0.090 ± 0.010	10	26
		50-60%	0.142 ± 0.003	0.317 ± 0.006	0.0040 ± 0.0004	12	26
		60-70%	0.140 ± 0.004	0.316 ± 0.005	0.019 ± 0.001	15	26
		70-80%	0.138 ± 0.005	0.313 ± 0.008	0.0083 ± 0.0003	18	26
	p	0-5%	0.149 ± 0.005	0.359 ± 0.008	4.38 ± 0.50	34	22
		5-10%	0.148 ± 0.004	0.348 ± 0.006	1.94 ± 0.30	36	22
		10-20%	0.146 ± 0.005	0.346 ± 0.006	0.80 ± 0.12	22	22
20-30%		0.145 ± 0.004	0.340 ± 0.007	0.33 ± 0.05	16	22	
30-40%		0.144 ± 0.004	0.335 ± 0.005	0.16 ± 0.03	8	22	
40-50%		0.144 ± 0.004	0.330 ± 0.006	0.078 ± 0.014	13	22	
50-60%		0.143 ± 0.004	0.300 ± 0.006	0.040 ± 0.005	1	22	
60-70%		0.139 ± 0.004	0.281 ± 0.005	0.017 ± 0.002	4	22	
70-80%		0.127 ± 0.004	0.274 ± 0.007	0.0080 ± 0.0006	10	22	

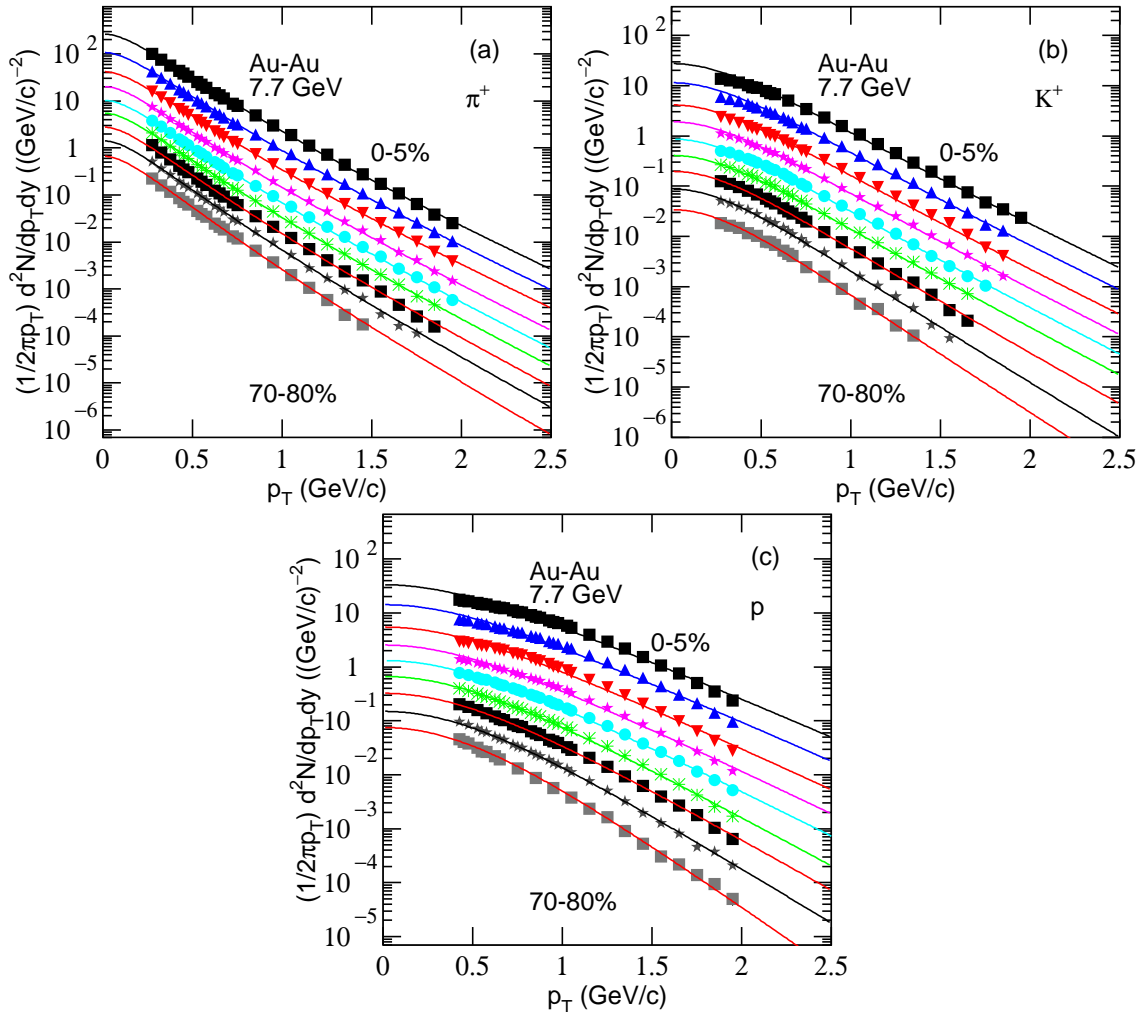


Fig. 1. Transverse momentum spectra of (a)-(c) π^+ , K^+ and p produced in different centrality bins in Au-Au collisions at $\sqrt{s_{NN}} = 7.7$ GeV. The symbols represent the experimental data measured by the STAR Collaboration in the mid-rapidity interval $|y| < 0.1$ [19]. The curves are our fitted results by Eq. (1). The ratios of Data/Fit corresponding to the panels (a)-(c) are presented by panels (a*)-(c*) respectively.

different event centralities. The symbols represent the parameter values averaged by weighting the yields of different particles which are listed in Table 1. One can see that T_0 and β_T increase with the increase of $\sqrt{s_{NN}}$ from 7.7 to 39 GeV. Meanwhile, T_0 and β_T increase with the increase of event centrality from periphery to center.

In addition, the variation of weight averages T_0 on β_T for different collision energies and event centralities are displayed in Fig. 7(c), where the symbols represent the parameter values averaged by weighting the yields of different particles. One can see that T_0 increases with the increase of β_T . At higher energy and in central collisions, one see larger T_0 and β_T . There is a positive correlation between T_0 and β_T .

The dependences of mean transverse momentum

($\langle p_T \rangle$) and initial temperature ($T_i = \sqrt{\langle p_T^2 \rangle} / 2$ [51, 52, 53]) on $\sqrt{s_{NN}}$ for different event centralities obtained by weighting the yields of different particles are shown in Figs. 8(a) and 8(b) respectively. One can see that $\langle p_T \rangle$ and T_i increase with the increase of $\sqrt{s_{NN}}$ from 7.7 to 39 GeV. Meanwhile, $\langle p_T \rangle$ and T_i increase with the increase of event centrality from periphery to center.

The reason for increasing of T_0 and β_T with the increase of collision energy is due to the fact that more energies are deposited in collisions at higher energy in the considered RHIC-BES energy range. Meanwhile, the system size at higher energy decreases due to relativistic constriction effect, which results in a smaller volume, then a larger energy density and larger T_0 . Meanwhile, at higher energy, the squeeze is more violent, which re-

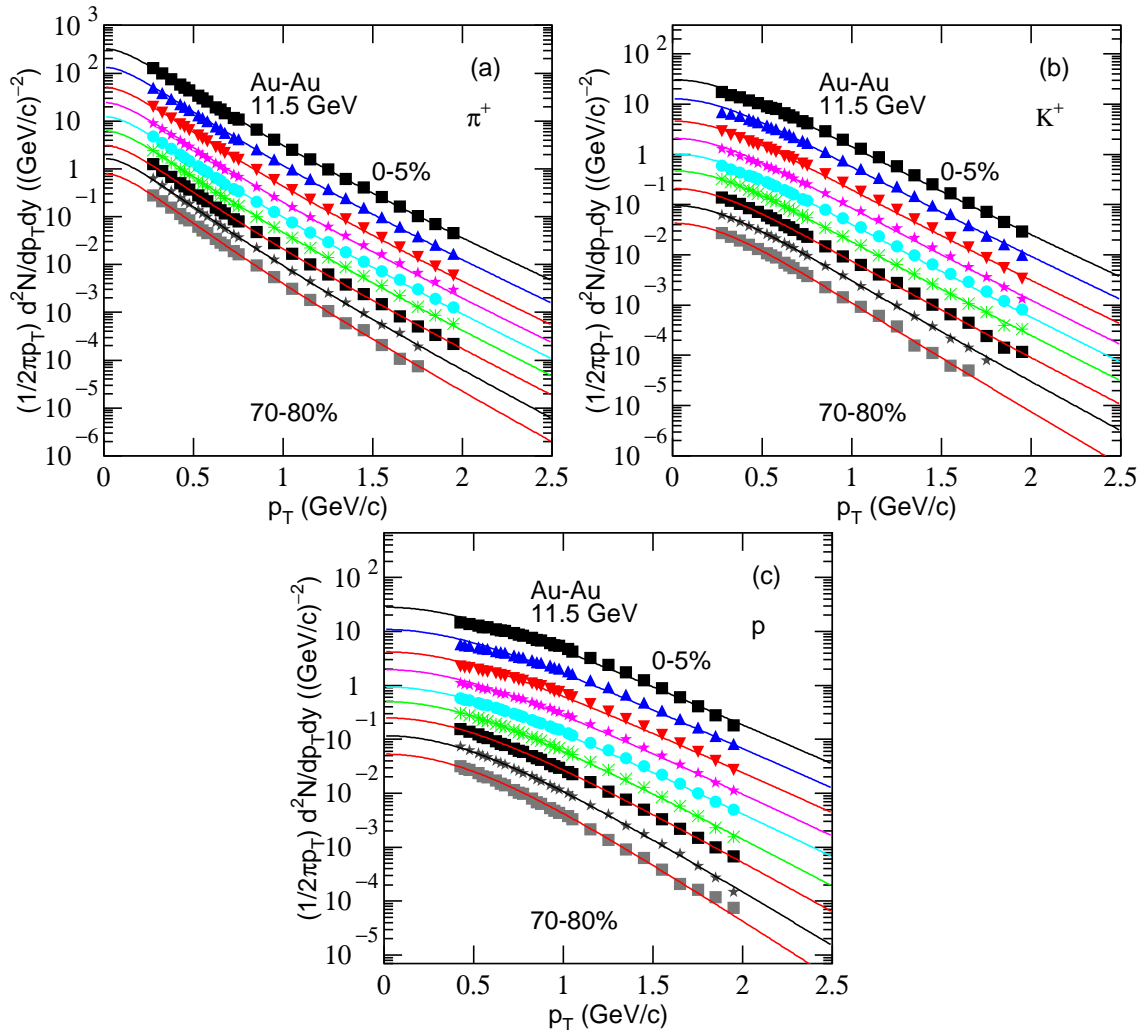


Fig. 2. The same as Fig. 1, but showing the results at $\sqrt{s_{NN}} = 11.5$ GeV.

sults in a rapider expansion and larger β_T .

The reason for increasing of T_0 and β_T with the increase of event centrality is due to the fact that the central collisions contain more nucleons than the peripheral collisions, then more energies are deposited in central collisions. Meanwhile a rapider expansion appears due to more violent squeeze in central collisions, comparatively to peripheral collisions. As a result, T_0 and β_T in central collisions are larger than those in peripheral collisions.

Because of $\langle p_T \rangle$ and T_i being positive correlation with T_0 and β_T , the increasing of T_0 and β_T with the increases of collision energy and event centrality result naturally in the increasing of $\langle p_T \rangle$ and T_i with the increases of collision energy and event centrality. This work shows that the two free parameters T_0 and β_T and the two derived parameters $\langle p_T \rangle$ and T_i ap-

pear similar law on the dependences of collision energy and event centrality. In particular, $\langle p_T \rangle$ and T_i are model-independent, though we obtain them from model-dependent free parameters T_0 and β_T in this work. In fact, $\langle p_T \rangle$ and T_i can be obtained by the p_T data themselves if the data are across the possible p_T range.

It should be noted that there is entanglement in the extraction of T_0 and β_T . In fact, if one uses a smaller T_0 and a larger β_T for central collisions, a decreasing trend for T_0 from peripheral to central collisions can be obtained. Meanwhile, a negative correlation between T_0 and β_T can also be obtained. Thus, this situation is in agreement with some current references [19, 54, 55]. If one even uses an almost invariant or slightly larger T_0 and a properly larger β_T for central collisions, an almost invariant or slightly increase trend for T_0 from peripheral to central collisions can be obtained [56]. To show

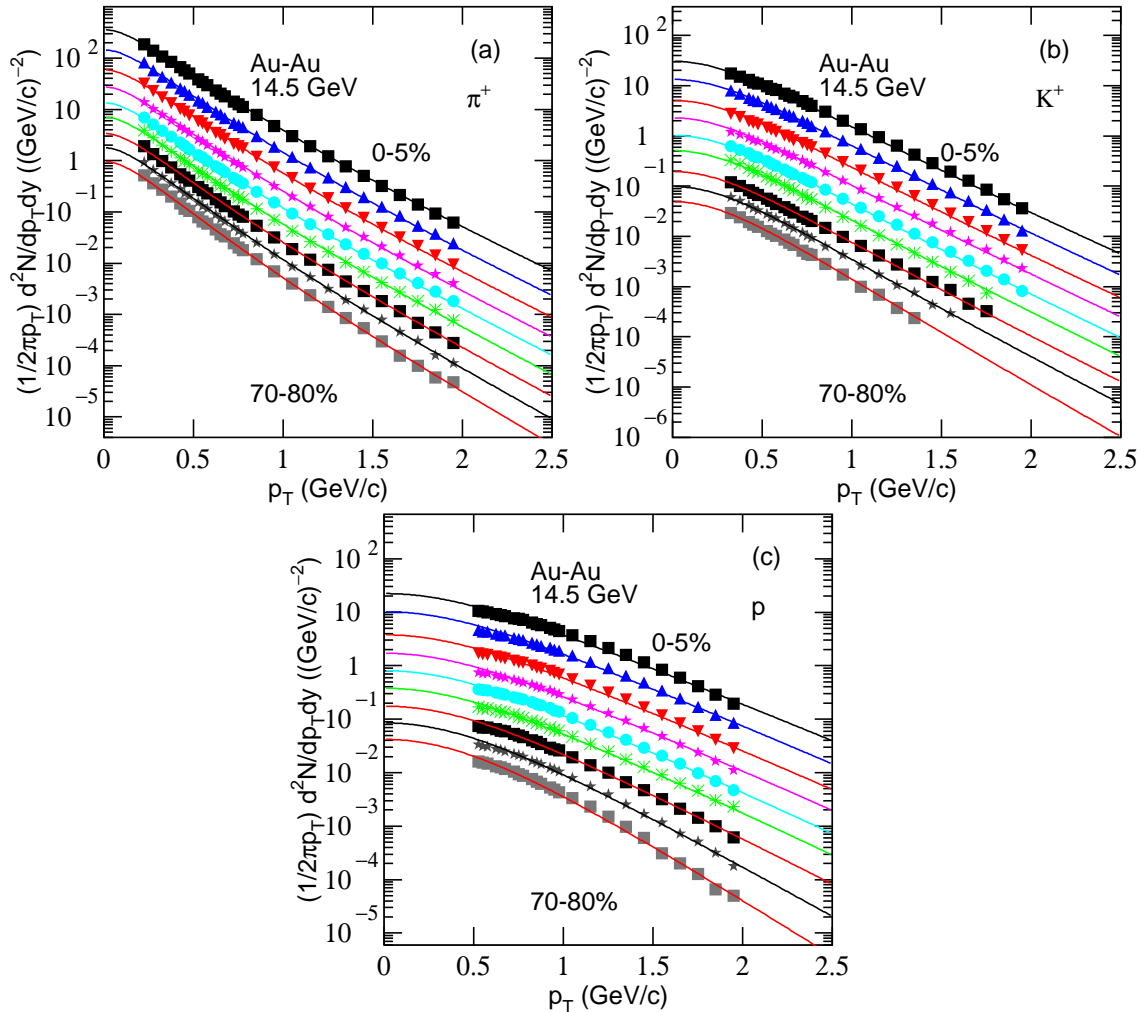


Fig. 3. The same as Fig. 1, but showing the results at $\sqrt{s_{NN}} = 14.5$ GeV, where the data are cited from ref. [20].

the flexibility in the extraction of T_0 and β_T , this work has reported an increasing trend for T_0 from peripheral to central collisions, and a positive correlation between T_0 and β_T .

This whole phenomenal analysis results in degree of thermal motion and collective expansion, that are reflected by T_0 and β_T . With the increasing collision energy, the system may undergo different evolution processes. In the considered RHIC-BES energy range, the violent degree of collisions increase with increasing the collision energy. The trends of T_0 and β_T show approximately monotonous increase in which large fluctuation does not appear. The evolution processes at the considered six energies show similar behaviors to each other.

4 Conclusions

The main observations and conclusions are summa-

rized here.

(a) Based on the data-driven analysis, the blast-wave model with Boltzmann-Gibbs statistics is used to analyze the collision energy dependent and event centrality dependent double-differential transverse momentum spectra of charged particles (π^+ , K^+ and p) produced in the mid-rapidity interval in Au-Au collisions at the RHIC-BES energies. The contribution of soft excitation is considered in this work, but the contribution of hard process is not excluded if available.

(b) As the free parameters, the kinetic freeze-out temperature T_0 and transverse flow velocity β_T are extracted by the blast-wave model. Both T_0 and β_T increase with the increase of collision energy due to more violent collisions at higher energy. The two parameters also increase with the increase of centrality, as the central collisions contain more nucleons which means more energy deposited and more violent collisions and

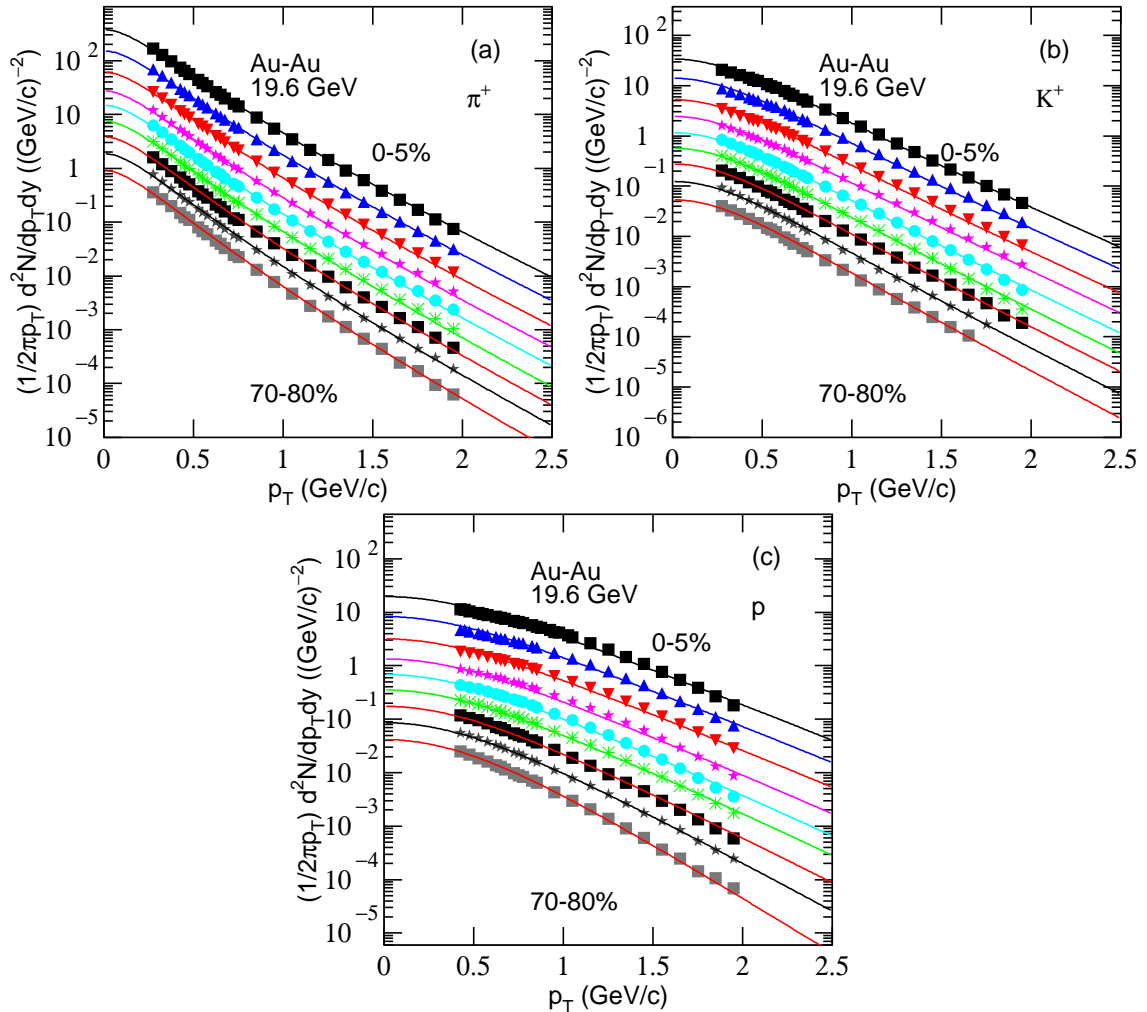


Fig. 4. The same as Fig. 1, but showing the results at $\sqrt{s_{NN}} = 19.6$ GeV.

squeeze, comparing with peripheral collisions.

(c) As the derived parameters, the mean transverse momentum $\langle p_T \rangle$ and initial temperature T_i appear similar law to the free parameters T_0 and β_T when we study the dependences of parameters on collision energy and event centrality. Although T_0 and β_T are model-dependent, $\langle p_T \rangle$ and T_i are generally model-independent. There is no large fluctuation in the excitation function of the considered parameters at the RHIC-BES, which means similar collision mechanism.

Acknowledgments

We thank Dr. Muhammad Usman Ashraf for his kind help. This work was supported by the National Natural Science Foundation of China under Grant No. 11575103, the Chinese Government Scholarship (China Scholarship Council), the Scientific and Technological

Innovation Programs of Higher Education Institutions in Shanxi (STIP) under Grant No. 201802017, the Shanxi Provincial Natural Science Foundation under Grant No. 201701D121005, and the Fund for Shanxi “1331 Project” Key Subjects Construction.

Data availability

The data used to support the findings of this study are included within the article and are cited at relevant places within the text as references.

Compliance with Ethical Standards

The authors declare that they are in compliance with ethical standards regarding the content of this paper.

Conflict of Interest

The authors declare that there are no conflicts of interest regarding the publication of this paper. The

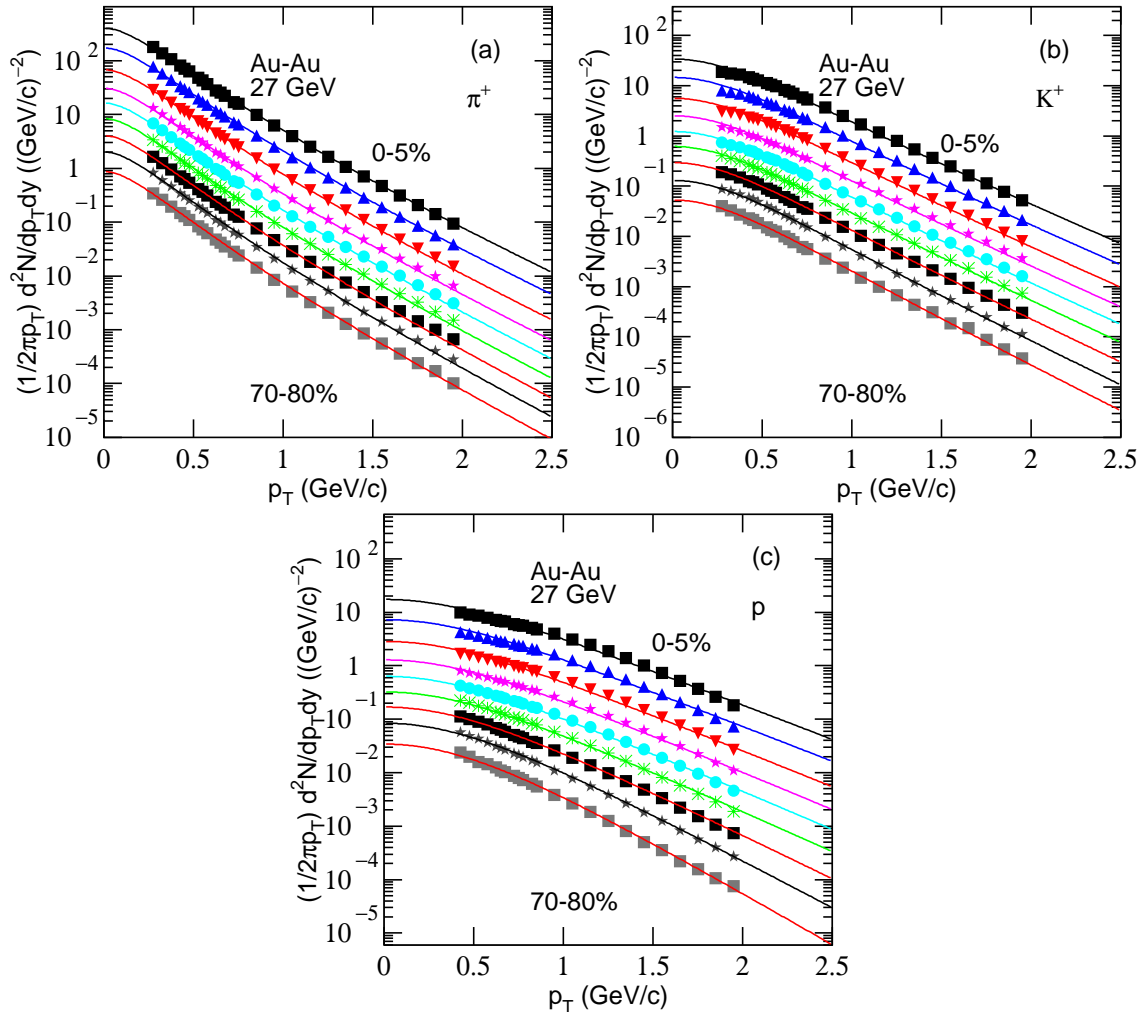


Fig. 5. The same as Fig. 1, but showing the results at $\sqrt{s_{NN}} = 27$ GeV.

funders had no role in the design of the study; in the collection, analyses, or interpretation of the data; in the writing of the manuscript, or in the decision to publish the results.

References

- [1] S. Mukherjee and V. Skokov, “Universality driven analytic structure of QCD crossover: Radius of convergence in baryon chemical potential,” arXiv:1909.04639 [hep-ph].
- [2] W.-J. Fu, J. M. Pawłowski, and F. Rennecke, “The QCD phase structure at finite temperature and density,” arXiv:1909.02991 [hep-ph].
- [3] G.-Y. Shao, W.-B. He, and X.-Y. Gao, “Deformed QCD phase structure and entropy oscillation in the presence of a magnetic background,” Phys. Rev. D **100**, 014020 (2019), doi:10.1103/PhysRevD.100.014020.
- [4] R. Sahoo, “Possible formation of QGP-droplets in proton-proton collisions at the CERN Large Hadron Collider,” AAPPs Bull. **29**(4), 16(2019), doi:10.22661/AAPPsBL.2019.29.4.16.
- [5] M. Gyulassy and L. McLerran, “New forms of QCD matter discovered at RHIC,” Nucl. Phys. A **750**, 30 (2005), doi:10.1016/j.nuclphysa.2004.10.034.
- [6] M. T. AlFiky, O. T. ElSherif, and A. M. Hamed, “Quark gluon plasma formation in proton-proton collisions using PYTHIA,” arXiv:1902.05114 [hep-ex].
- [7] F. Rennecke, W.-J. Fu, and J. M. Pawłowski, “Strangeness neutrality and the QCD phase diagram,” arXiv:1907.08179 [hep-ph].
- [8] A. Andronic, P. Braun-Munzinger, and J. Stachel, “Hadron production in central nucleus-nucleus collisions at chemical freeze-out,” Nucl. Phys. A **772**, 167 (2006), doi:10.1016/j.nuclphysa.2006.03.012.

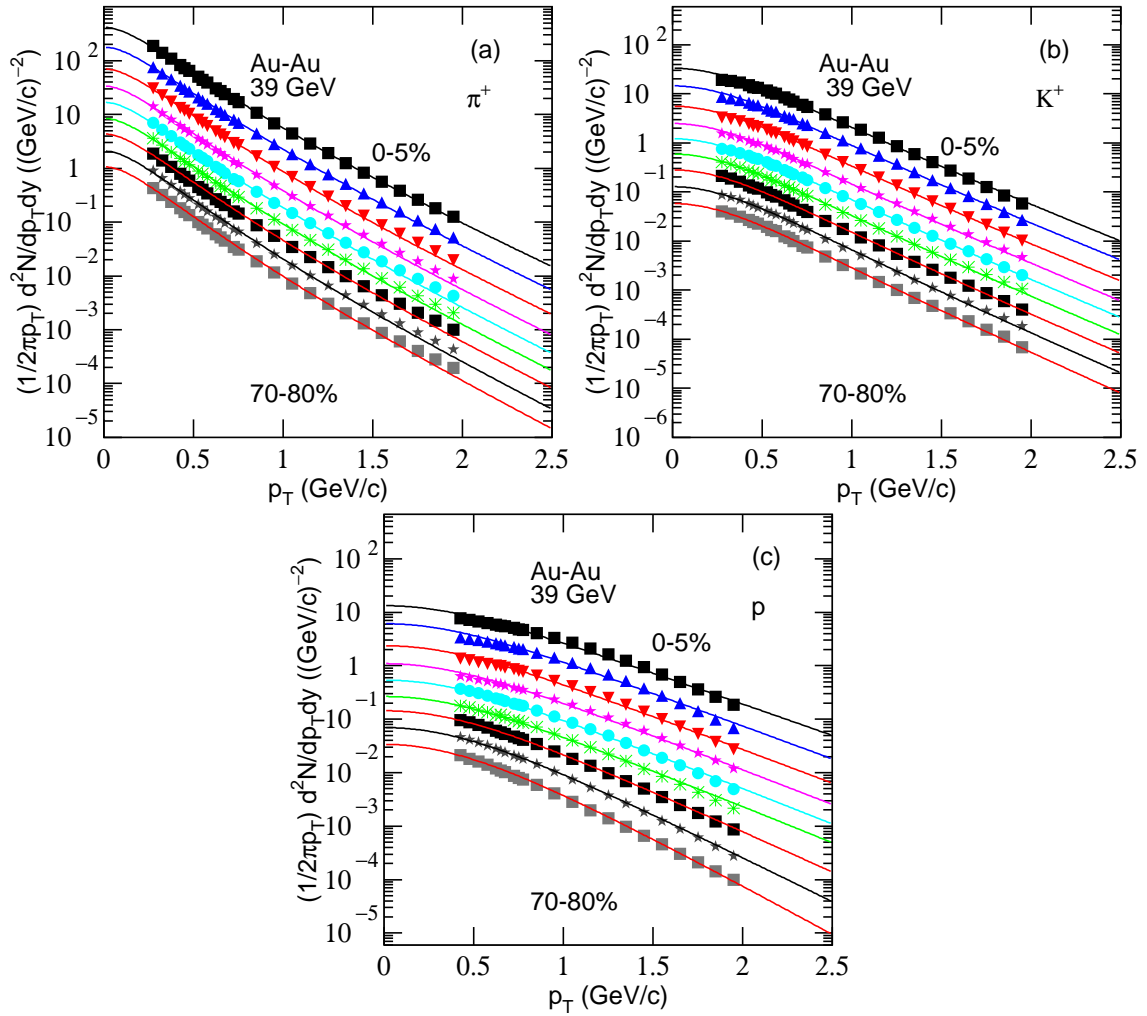


Fig. 6. The same as Fig. 1, but showing the results at $\sqrt{s_{NN}} = 39$ GeV.

- [9] G. Inghirami, P. Hillmann, B. Tomášik, and M. Bleicher, “Temperatures and chemical potentials at kinetic freeze-out in relativistic heavy ion collisions from coarse grained transport simulations,” arXiv:1909.00643 [hep-ph].
- [10] C. Yang for the STAR Collaboration, “The STAR detector upgrades and physics in beam energy scan phase II,” EPJ Web Conf. **182**, 02130 (2018), doi:10.1051/epjconf/201818202130.
- [11] K. C. Meehan for the STAR Collaboration, “Fixed target collisions at STAR,” Nucl. Phys. A **956**, 878 (2016), doi:10.1016/j.nuclphysa.2016.04.016.
- [12] X. Sun for the STAR Collaboration, “Flow in the RHIC Beam Energy Scan from STAR,” J. Phys. Conf. Ser. **535**, 012005 (2014), doi:10.1088/1742-6596/535/1/012005.
- [13] K. C. Meehan for the STAR Collaboration, “The fixed-target experiment at STAR,” J. Phys. Conf. Ser. **742**, 012022 (2016), doi:10.1088/1742-6596/742/1/012022.
- [14] T. Abyazimov et al. (CBM Collaboration), “Challenges in QCD matter physics – The scientific programme of the Compressed Baryonic Matter experiment at FAIR,” Eur. Phys. J. A **53**, 60 (2017), doi:10.1140/epja/i2017-12248-y.
- [15] J. Chen, D. Keane, Y. G. Ma, A. Tang, and Z. Xu, “Antinuclei in heavy-ion collisions,” Phys. Rept. **760**, 1 (2018), doi:10.1016/j.physrep.2018.07.002.
- [16] N. Xu for the STAR Collaboration, “An overview of STAR experimental results,” Nucl. Phys. A **931**, 1 (2014), doi:10.1016/j.nuclphysa.2014.10.022.
- [17] S. Chatterjee, S. Das, L. Kumar, D. Mishra, B. Mohanty, R. Sahoo, and N. Sharma, “Freeze-out parameters in heavy-ion collisions at AGS, SPS, RHIC, and LHC energies,” Adv. High Energy Phys. **2015**, 349013 (2015), doi:10.1155/2015/349013.
- [18] S. Uddin, I. Bashir, and R. A. Bhat, “Transverse momentum distributions of hadrons produced in Pb-Pb collisions at LHC energy $\sqrt{s_{NN}} = 2.76$ TeV,”

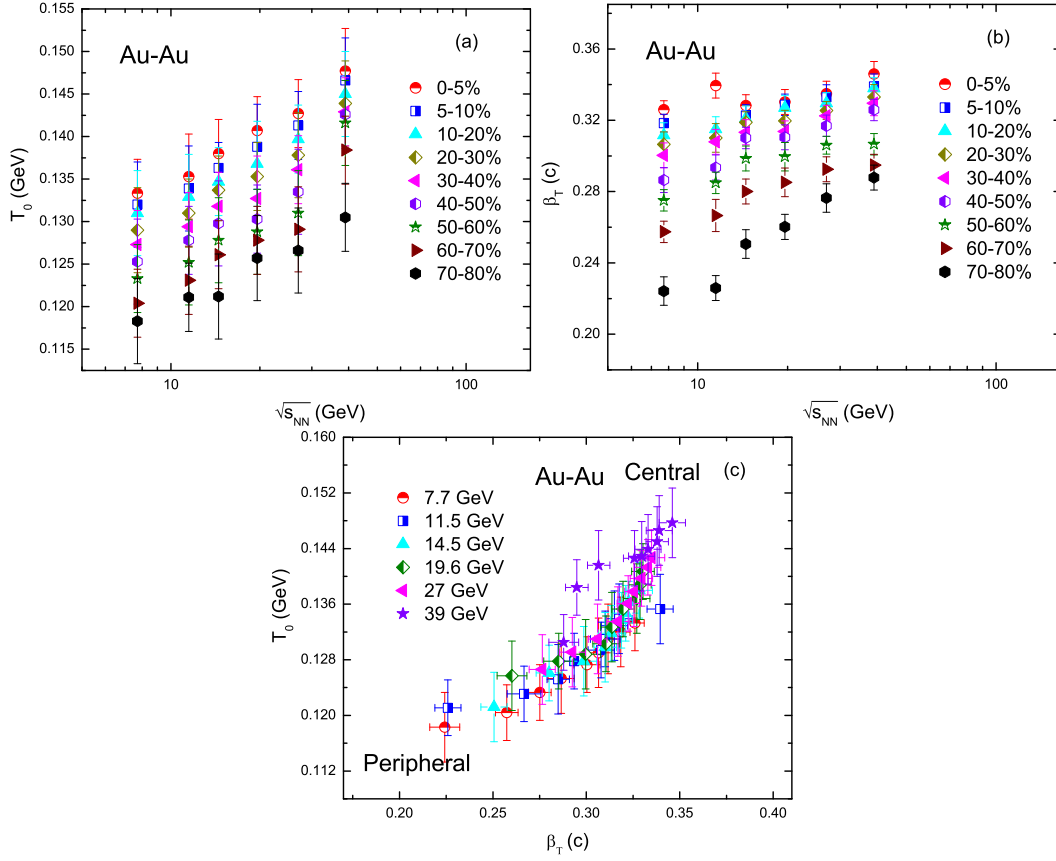


Fig. 7. Dependences of weight averages (a) T_0 and (b) β_T on $\sqrt{s_{NN}}$ for different event centralities as well as (c) T_0 on β_T for different collision energies and event centralities. The different symbols display different centrality classes in Figs. 7(a) and 7(b) or different collision energies in Fig. 7(c), which are averaged by weighting the yields of different particles which are listed in Table 1.

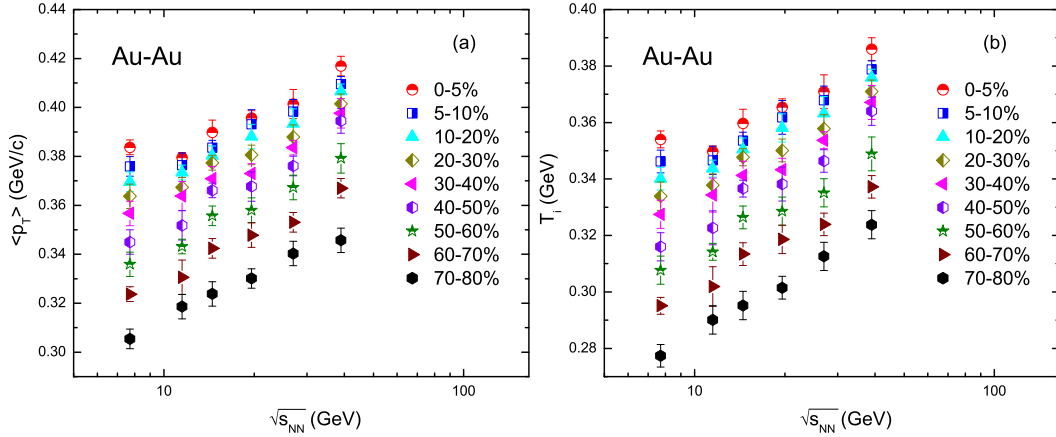


Fig. 8. Dependences of weight averages (a) $\langle p_T \rangle$ and (b) T_i on $\sqrt{s_{NN}}$ for different event centralities. The different symbols display different centrality classes, which are averaged by weighting the yields of different particles which are listed in Table 1.

- itc heavy ion collisions from the Beam Energy Scan program,” *Phys. Rev. C* **96**, 044904 (2017), doi:10.1103/PhysRevC.96.044904.
- [20] V. Bairathi for the STAR Collaboration, “Study of the bulk properties of the system formed in Au+Au collisions at $\sqrt{s_{NN}} = 14.5$ GeV using the STAR detector at RHIC,” *Nucl. Phys. A* **956**, 292 (2016), doi:10.1016/j.nuclphysa.2016.02.066.
- [21] E. Schnedermann, J. Sollfrank, and U. Heinz, “Thermal phenomenology of hadrons from 200 A GeV S+S collisions,” *Phys. Rev. C* **48**, 2462 (1993), doi:10.1103/PhysRevC.48.2462.
- [22] B. I. Abelev et al. (STAR Collaboration), “Systematic measurements of identified particle spectra in pp, d+Au and Au+Au collisions from STAR,” *Phys. Rev. C* **79**, 034909 (2009), doi:10.1103/PhysRevC.79.034909.
- [23] B. I. Abelev et al. (STAR Collaboration), “Identified particle production, azimuthal anisotropy, and interferometry measurements in Au+Au collisions at $\sqrt{s_{NN}} = 9.2$ GeV,” *Phys. Rev. C* **81**, 024911 (2010), doi:10.1103/PhysRevC.81.024911.
- [24] Z. B. Tang, Y. C. Xu, L. J. Ruan, G. van Buren, F. Q. Wang, and Z. B. Xu, “Spectra and radial flow in relativistic heavy ion collisions with Tsallis statistics in a blast-wave description,” *Phys. Rev. C* **79**, 051901(R) (2009), doi:10.1103/PhysRevC.79.051901.
- [25] Z. B. Tang, L. J. Ruan, M. Shao, H. F. Chen, C. Li, B. Mohanty, P. Sorensen, A. H. Tang, and Z. B. Xu, “Statistical origin of constituent-quark scaling in the QGP hadronization,” *Chin. Phys. Lett.* **30**, 031201 (2013), doi:10.1088/0256-307X/30/3/031201.
- [26] K. Jiang, Y. Y. Zhu, W. T. Liu, H. F. Chen, C. Li, L. J. Ruan, M. Shao, Z. B. Tang, and Z. B. Xu, “Onset of radial flow in p+p collisions,” *Phys. Rev. C* **91**, 024910 (2015), doi:10.1103/PhysRevC.91.024910.
- [27] S. Takeuchi, K. Murase, T. Hirano, P. Huovinen, and Y. Nara, “Effects of hadronic rescattering on multistrange hadrons in high energy nuclear collisions,” *Phys. Rev. C* **92**, 044907 (2015), doi:10.1103/PhysRevC.92.044907.
- [28] H. Hiesengerg and A. M. Levy, “Elliptical flow and Hanbury-Brown-Twiss correlations in noncentral nuclear collisions,” *Phys. Rev. C* **59**, 2716 (1999), doi:10.1103/PhysRevC.59.2716.
- [29] U. W. Heinz, *Lecture Notes for Lectures Presented at the 2nd CERN-Latin-American School of High-Energy Physics*, 1–14 June 2003, San Miguel Regla, Mexico, arXiv:hep-ph/0407360 (2004).
- [30] R. Russo, *Measurement of D^+ meson production in p-Pb collisions with the ALICE detector*, PhD Thesis, Universita degli Studi di Torino, Italy, arXiv:1511.04380 [nucl-ex] (2015).
- [31] S. Sadhu and P. Ghosh, “Anomalous features of particle production in high-multiplicity events of pp collisions at the LHC energies,” *Phys. Rev. D* **99**, 034020 (2019), doi:10.1103/PhysRevD.99.034020.
- [32] G. Bíró, G. G. Barnafódi, T. S. Biró, K. Ürmösy, and Á. Takács, “Systematic analysis of the non-extensive statistical approach in high energy particle collisions - Experiment vs. theory,” *Entropy* **19**, 88 (2017), doi:10.3390/e19030088.
- [33] H.-R. Wei, F.-H. Liu, and R. A. Lacey, “Disentangling random thermal motion of particles and collective expansion of source from transverse momentum spectra in high energy collisions,” *J. Phys. G* **43**, 125102 (2016), doi:10.1088/0954-3899/43/12/125102.
- [34] H.-R. Wei, F.-H. Liu, and R. A. Lacey, “Kinetic freeze-out temperature and flow velocity extracted from transverse momentum spectra of final-state light flavor particles produced in collisions at RHIC and LHC,” *Eur. Phys. J. A* **52**, 102 (2016), doi:10.1140/epja/i2016-16102-6.
- [35] H.-L. Lao, H.-R. Wei, F.-H. Liu, and R. A. Lacey, “An evidence of mass-dependent differential kinetic freeze-out scenario observed in Pb-Pb collisions at 2.76 TeV,” *Eur. Phys. J. A* **52**, 203 (2016), doi:10.1140/epja/i2016-16203-2.
- [36] H.-L. Lao, F.-H. Liu, B.-C. Li, and M.-Y. Duan, “Kinetic freeze-out temperatures in central and peripheral collisions: which one is larger?,” *Nucl. Sci. Tech.* **29**, 82 (2018), doi:10.1007/s41365-018-0425-x.
- [37] H.-L. Lao, F.-H. Liu, B.-C. Li, M.-Y. Duan, R. A. Lacey, “Examining the model dependence of the determination of kinetic freeze-out temperature and transverse flow velocity in small collision system,” *Nucl. Sci. Tech.* **29**, 164 (2018), doi:10.1007/s41365-018-0504-z.
- [38] J. Cleymans and D. Worku, “Relativistic thermodynamics: transverse momentum distributions in high-energy physics,” *Eur. Phys. J. A* **48**, 160 (2012), doi:10.1140/epja/i2012-12160-0.
- [39] H. Zheng and L. L. Zhu, “Comparing the Tsallis distribution with and without thermodynamical description in p+p collisions,” *Adv. High Energy Phys.* **2016**, 96321126 (2016). <http://doi/10.1155/2016/9632126>
- [40] R. Hagedorn, “Multiplicities, p_T distributions and the expected hadron \rightarrow quark-gluon phase transition,” *Riv. Nuovo Cimento*, **6**(10), 1 (1983), <https://doi.org/10.1007/BF02740917>.
- [41] B. B. Abelev et al. (ALICE Collaboration), “Production of $\Sigma(1385)^\pm$ and $\Xi(1530)^0$ in proton-proton collisions at $\sqrt{s} = 7$ TeV,” *Eur. Phys. J. C* **75**, 1 (2015), doi:10.1140/epjc/s10052-014-3191-x.
- [42] R. L. Ray and A. Jentsch, “Phenomenological models of two-particle correlations on transverse momentum in relativistic heavy-ion collisions,” *Phys. Rev. C* **99**, 024911 (2019), doi:10.1103/PhysRevC.99.024911.
- [43] S. Chatrchyan et al. (CMS Collaboration), “Study of high- p_T charged particle suppression in PbPb compared

- to pp collisions at $\sqrt{s_{NN}} = 2.76$ TeV,” *Eur. Phys. J. C* **72**, 1945 (2012), doi:10.1140/epjc/s10052-012-1945-x.
- [44] C. Tsallis, “Possible generalization of Boltzmann-Gibbs statistics,” *J. Stat. Phys.* **52**, 479 (1988), doi:10.1007/BF01016429.
- [45] B. I. Abelev et al. (STAR Collaboration), “Strange particle production in p+p collisions at $\sqrt{s_{NN}} = 200$ GeV,” *Phys. Rev.C* **75**, 064901 (2007), doi:10.1103/PhysRevC.75.064901.
- [46] T. S. Biró, G. Purcsel, and K. Ürmössy, “Non-extensive approach to quark matter,” *Eur. Phys. J. A* **40**, 325 (2009), doi:10.1140/epja/i2009-10806-6.
- [47] R. Odorico, “Does a transverse energy trigger actually trigger on large- p_T jets?,” *Phys. Lett. B* **118**, 151 (1982), doi:10.1016/0370-2693(82)90620-7.
- [48] G. Arnison et al. (UA1 Collaboration), “Transverse momentum spectra for charged particles at the CERN proton-antiproton collider,” *Phys. Lett. B* **118**, 167 (1982), doi:10.1016/0370-2693(82)90623-2.
- [49] T. Mizoguchi, M. Biyajima, and N. Suzuki, “Analyses of whole transverse momentum distributions in $p\bar{p}$ and pp collisions by using a modified version of Hagedorn’s formula,” *Int. J. Mod. Phys. A* **32**, 1750057 (2017), doi:10.1142/S0217751X17500579
- [50] M. K. Suleymanov, “The meaning behind observed p_T regions at the LHC energies,” *Int. J. Mod. Phys. E* **27**, 1850008 (2018), doi:10.1142/S0218301318500088.
- [51] L. G. Gutay, A. S. Hirsch, C. Pajares, R. P. Scharenberg, and B. K. Srivastava, “De-confinement in small systems: Clustering of color sources in high multiplicity $\bar{p}p$ collisions at $\sqrt{s} = 1.8$ TeV,” *Int. J. Mod. Phys. E* **24**, 1550101 (2015), doi:10.1142/S0218301315501013.
- [52] A. S. Hirsch, C. Pajares, R. P. Scharenberg, and B. K. Srivastava, “De-confinement in high multiplicity proton-proton collisions at LHC energies,” arXiv:1803.02301 [hep-ph] (2018).
- [53] P. Sahoo, S. De, S. K. Tiwari, and R. Sahoo, “Energy and centrality dependent study of deconfinement phase transition in a color string percolation approach at RHIC energies,” *Eur. Phys. J. A* **54**, 136 (2018), doi:10.1140/epja/i2018-12571-9.
- [54] B. Abelev et al. (ALICE Collaboration), “Centrality dependence of π , K , p production in Pb-Pb collisions at $\sqrt{s_{NN}} = 2.76$ TeV,” *Phys. Rev. C* **88**, 044910 (2013), doi:10.1103/PhysRevC.88.044910.
- [55] L. Kumar for the STAR Collaboration, “Systematics of kinetic freeze-out properties in high energy collisions from STAR,” *Nucl. Phys. A* **931**, 1114 (2014), doi:10.1016/j.nuclphysa.2014.08.085.
- [56] A. Khuntia, H. Sharma, S. K. Tiwari, R. Sahoo, and J. Cleymans, “Radial flow and differential freeze-out in proton-proton collisions at $\sqrt{s} = 7$ TeV at the LHC,” *Eur. Phys. J. A* **55**, 3 (2019), doi:10.1140/epja/i2019-12669-6.